Report
P-20-19
August 2020

EBS TF – THM modelling

Water transport in pellets-filled slots – modelling of test cases A and C

Mattias Åkesson

SVENSK KÄRNBRÄNSLEHANTERING AB

SWEDISH NUCLEAR FUEL
AND WASTE MANAGEMENT CO

Box 3091, SE-169 03 Solna
Phone +46 8 459 84 00
skb.se

SVENSK KÄRNBRÄNSLEHANTERING

ISSN 1651-4416
SKB P-20-19
ID 1900487

August 2020

EBS TF – THM modelling

Water transport in pellets-filled slots – modelling of test cases A and C

Mattias Åkesson, Svensk Kärnbränslehantering AB

Abstract

This report presents the modelling work performed within EBS Taskforce “Task 10 Water transport in pellets-filled slots”. The aim of this task was to investigate the ability of models (existing or new) to simulate water transport at different test conditions. Two subtasks have addressed two test types: A) 1D-tests with water freely available (water uptake tests), and C) 1D-tests with water redistribution in a temperature gradient. Tests were performed with two different pellets materials: extruded Asha NW BFL-L and roller compacted MX-80.

The calculations were performed with the FEM tool Code_Bright. The used material model included established constitutive relations: i) a van Genuchten type water retention curve; ii) the Darcy´s law for unsaturated liquid transport; and iii) vapour diffusion. Results show that the processes in Test A and C can be described with these relations.

Sammanfattning

Denna rapport presenterar ett modelleringsarbete som utförts inom samarbetsprojektet ”Task force on Engineered Barrier Systems” och Task 10 Vattentransport i pelletsfyllda spalter. Målet med denna modelleringsuppgift var att undersöka olika (befintliga eller nya) materialmodellers förmåga att simulera vattentransport under olika testförhållanden. Två deluppgifter har inriktats mot två testtyper: A) 1D-tester med fri tillgång på vatten (vattenupptagsförsök), och C) 1D-tester med fuktomfördelning i en temperaturgradient. Testerna utfördes med två olika pelletsmaterial: extruderad Asha NW BFL-L, och rullkompakterad MX-80.

Beräkningarna utfördes med hjälp av finita elementkoden Code_Bright. Den använda materialmodellen innefattade etablerade konstitutiva samband: i) en vattenretentionskurva av van Genuchten typ; ii) Darcy´s lag för omättad vätsketransport; samt iii) ångdiffusion. Resultaten visar att processerna i Test A och C kan beskrivas med dessa samband.

Contents

1 Introduction

This report presents the contribution from Clay Technology to the subtasks A and C of the modelling task "*Task 10. Water transport in pellets-filled slots*" organized within the EBS Taskforce.

The aim of the task was to formulate new models or (if available) use existing models for water transport in pellet fillings and to calibrate and check their ability to model water transport at different boundary and inflow conditions and at different temperature situations.

The subtasks A and C have addressed the following basic tests:

- A) 1D-tests with water freely available (water uptake tests).
- C) 1D-tests with water redistribution in a temperature gradient.

Both test types were performed in vertically oriented Plexiglas cylinders, 50 cm long and with an inner diameter of 10 cm, filled with the pellets material (see Figure 1-1). Tap water was available in a filter in the lower end of the cylinder used in the type A tests. In contrast, a temperature gradient was applied along the axis of the cylinder used in the type C tests, which were thermally insulated, heated at the bottom and cooled at the top. A detailed description of the different tests was presented by Åkesson et al. (2020). The tests were performed with two different pellets materials: extruded Asha NW BFL-L and roller compacted MX-80.

The approach for this modelling task has been to use the FEM code Code_Bright (v4) and to utilize the constitutive laws implemented in this, especially the implemented models for Darcy´s law for unsaturated condition, vapour diffusion and water retention properties. The thermal problem in subtask C was simplified as far as possible, and no mechanical processes were considered in any of the subtasks.

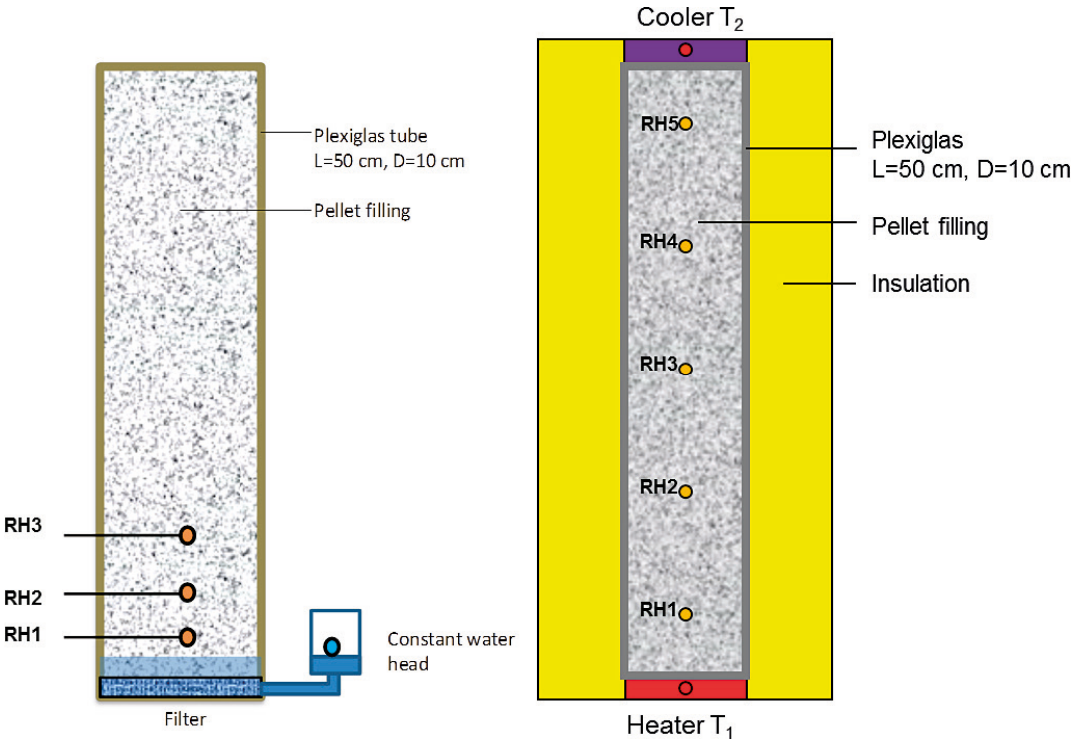

Figure 1-1. *Schematic drawings for the test arrangements for test type A (left) and C (right).*

A methodology for parameter value adoption was followed in which the experimental results from the analyzed tests were used as far as possible. However, independently determined water retention curves were also used for the test cases with MX-80.

A description of the model setup, with different model cases, parameter value adoption, geometry and conditions, is presented in Chapter 2. The model results are presented and compared with experimental results in Chapter 3. An analysis of the influence of vapour diffusion in Test A conditions is given in Chapter 4. The findings from the A and C tests is discussed in Chapter 5, and some concluding remarks is finally given in Chapter 6.

2 Model setup

2.1 Model cases

This analysis was performed with a set of model cases (Table 2-1) which were defined and implemented successively. The first step was to adopt relevant parameter values. These were based on the experimental results from the analysed tests themselves with the exception for the water retention curves for MX-80 bentonite, which were based on independent test data. The second step was to define base case models for each combination of bentonite material and test conditions: Test A was defined as a hydraulic process, whereas the Test C was defined as a thermohydraulic process. The third step was to define modified cases by which better agreements with experimental data could be pursued. For the A tests this involved i) the inclusion of vapour diffusion and ii) a rapid initial water uptake. For the C test it involved a controlled temperature field in the geometry. Since there was slightly different initial dry densities in the C tests with MX-80 (Cr3d and Cr3e), two models were implemented for both the base case and the modified case.

Table 2-1. Compilation of analysed model cases.

Step	Asha		MX-80	
Parameter values	Evaluated from A and C tests results		Evaluated from A tests results Water retention data	
Base case	Test A H model *Asha_case_6*	Test C TH model *Asha_case_7*	Test A H model *MX-80_Hmod_1*	Test C (d & e) TH model *MX-80_90d_1* *MX-80_1year_1*
Modified cases	TH model (vapour) *Asha_case_5* Initial water uptake *Asha_5_4*	Controlled temperature *Asha_7_3*	TH model (vapour) *MX-80_IT_2* Initial water uptake *MX-80_IT_2_3*	Controlled temperature *MX-80_90d_5* *MX-80_1year_2*

2.2 Evaluation of material properties

2.2.1 Approach

The methodology for parameter value adoption is schematically illustrated in Figure 2-1 and essentially consisted of five steps.

First, the water content distributions obtained from the Type A tests were used to adopt a *moisture diffusivity* value. This is a consequence of the fact that the water uptake can be described as following Fick´s second law ($\partial w/\partial t = D \cdot \Delta w$) under the assumption that the porosity is homogeneous throughout the test volume. Moreover, if the moisture diffusivity (D) is regarded as a constant, then the analytical solutions for diffusion in a plane sheet, with uniform initial distribution and equal surface concentrations (Crank 1975) can be used to describe the water content distributions at different times.

Second, the final readings from the RH sensors and the measured water content values representative for the sensor positions in the Type C tests were used to adopt a *water retention curve*. For MX-80, however, this was complemented with independent data from the literature.

Third, the moisture diffusivity value and the water retention curve were used to adopt a saturation-dependent permeability relation. This is a consequence of the fact that the moisture flux is proportional to the gradient of any moisture state variable and that the flow coefficient for this depends on the moisture state, which means that one can always (under isothermal conditions) evaluate a flow coefficient for another moisture state variable.

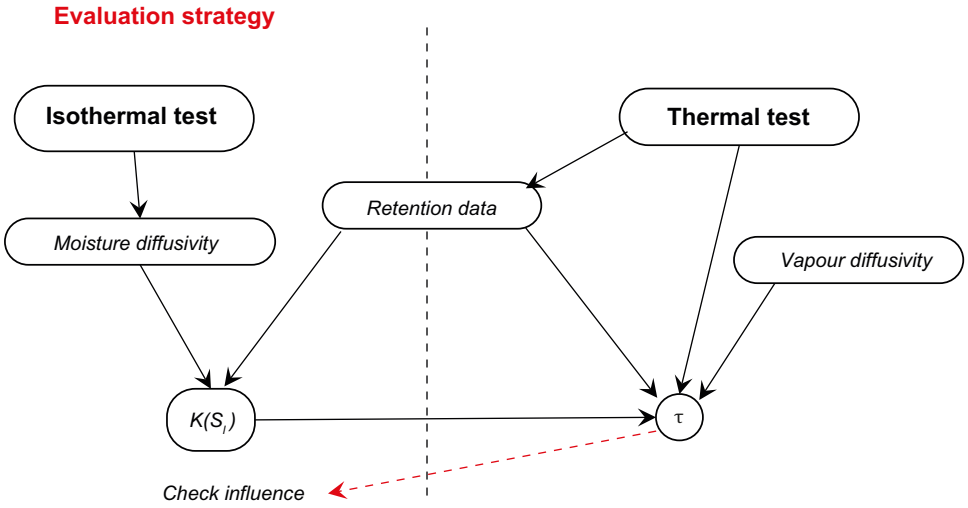

Figure 2-1. *Schematic illustration of the methodology for parameter value adoption.*

Fourth, the saturation-dependent permeability relation and the water retention curve were used to simulate the moisture redistribution process of the Type C tests. The time-scale for this redistribution and to some extent the steady-state water content profile can be used to adjust the vapour diffusion tortuosity value.

Finally, the potential contribution of vapour diffusion on the water transport in the Type A tests was investigated.

2.2.2 Moisture diffusivity evaluations

Water content distributions obtained from the Type A tests were used to adopt moisture diffusivity values. This was made through comparison of the experimental data with the analytical solution (Crank 1975):

$$\frac{w - w_i}{w_{bc} - w_i} = 1 - \frac{4}{\pi}\sum_{n=0}^{\infty}\frac{(-1)^n}{2n+1}\exp\left(-D(2n+1)^2\frac{\pi^2 t}{4L^2}\right)\cos\left(\frac{(2n+1)\pi x}{2L}\right) \qquad (2\text{-}1)$$

This describes the distribution of the water content (w) as a function of time (t) and the distance from the closed boundary (x). L is the length 0.5 m. The initial water content (w_i) and the boundary water content (w_{bc}) used in the evaluations is given in Table 2-2. The latter values were derived from the void ratio values for the pellet materials.

The diffusivity values for the two materials were fitted by hand in order to approximate the experimental data from three tests for each material as good as possible (Figure 2-2). In this way the diffusivity values for the MX-80 and the Asha pellets was found to be 2.7×10^{-10} and 4.0×10^{-10} m^2/s, respectively.

Table 2-2. Initial and boundary water contents.

	Initial water content (%)	Boundary water content (%)
MX-80	15.0	69.1
Asha	15.6	70.2

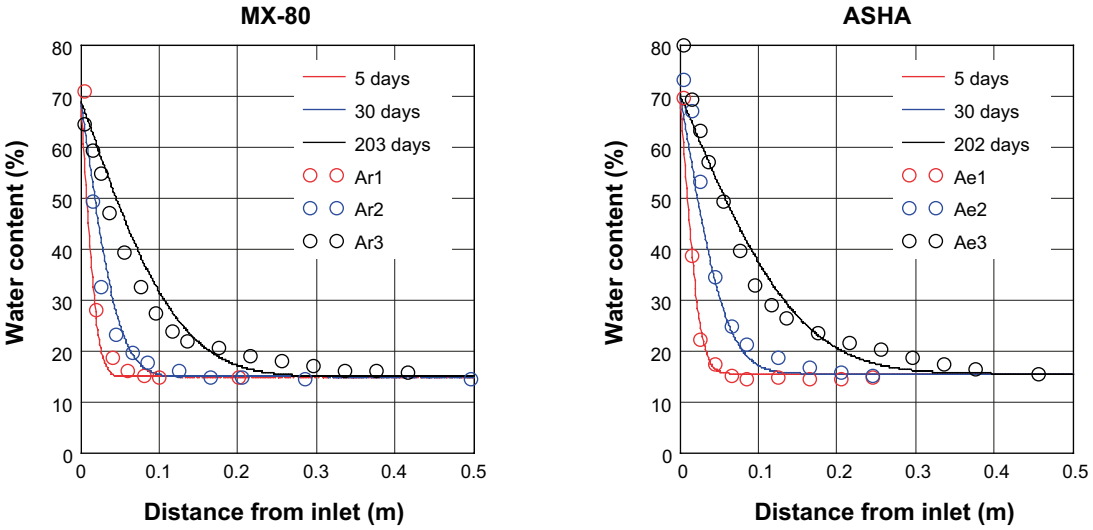

Figure 2-2. *Adoption of moisture diffusivity values from Type A test results.*

2.2.3 Asha extruded pellets

The parameter value adoption was based on the evaluated moisture diffusivity value described in the previous section and a water retention curve.

For the Asha pellets, a water retention curve was adopted by evaluating the final readings from the RH sensors and the measured water content values representative for the sensor positions in the Type C test Ce3d. The final RH (and temperature) readings were converted to suction values using Kelvin´s law, whereas the water contents were converted to degrees of saturation by assuming a constant void ratio. These five points are shown in Figure 2-3. In addition, a swelling pressure curve, derived for MX-80 by Åkesson et al. (2010), is also shown. Based on this data, a so-called extended van-Genuchten curve was adopted:

$$S_l(s) = \left[1 + \left(\frac{s}{P_0}\right)^{\frac{1}{1-\lambda_0}}\right]^{-\lambda_0} \cdot \left(1 - \frac{s}{P_d}\right)^{\lambda_d} \qquad (2\text{-}2)$$

The following parameter values were evaluated: $P_0 = 0.06$ MPa; $\lambda_0 = 0.17$; $P_d = 500$ MPa; and $\lambda_d = 1$.

From the diffusivity value and the water retention curve, a saturation dependent permeability relation was adopted on the following form:

$$k(S_l) = k_0 \cdot S_l^{\gamma} \qquad (2\text{-}3)$$

This adoption was based on the relation between the moisture diffusivity (D_l), permeability (k), porosity (n), viscosity (μ) and the derivative of the water retention curve:

$$D_l(S_l) = \frac{k(S_l)}{n \cdot \mu} \cdot \frac{dP_l}{dS_l} \qquad (2\text{-}4)$$

The permeability relation was calibrated by hand so that the resulting diffusivity relation exhibited a plateau at the sought level of 4.0×10^{-10} m^2/s (Figure 2-3, right). This was obtained with the parameter values $k_0 = 8 \times 10^{-19}$ m^2; and $\gamma = 5.7$.

All evaluated parameter values are compiled in Table 2-3. In addition, a thermal conductivity with a linear saturation dependence was adopted from Åkesson et al. (2010). A vapour diffusion tortuosity value of 0.5 was guessed and was found to give results in good agreement with the experimental data. The particle density value was taken from the task definition. For the water density, a reference value of 1 000 kg/m^3 was used together with a thermal expansion value used as default value in Code_Bright and a very low compressibility value. Finally, an initial liquid pressure value of −64 MPa was adopted which corresponds to the initial water content of the Ce3d test (14.7 %).

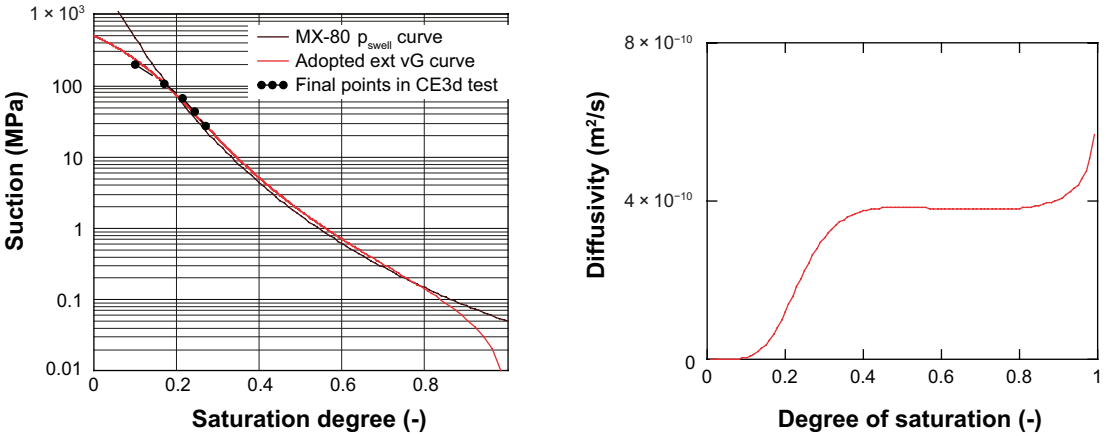

Figure 2-3. Adoption of water retention curve for Asha pellets (left). Effective moisture diffusivity relation for Asha pellets, after calibration of permeability relation (right).

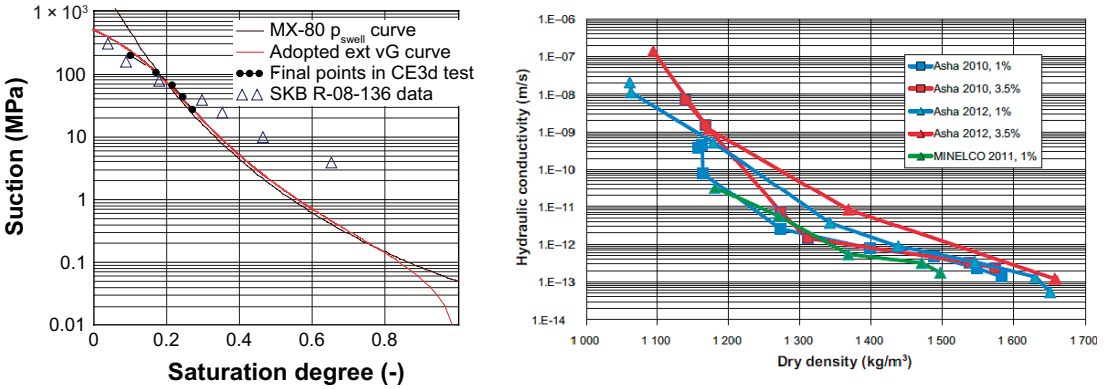

Figure 2-4. Water retention curves for Asha material, evaluated in this study and Johannesson et al. 2008 (left). Hydraulic conductivity versus dry density for Asha material and different salt contents Sandén et al. (2014) (right).

Table 2-3. Compilation of parameter values for different pellets material.

Parameter	Asha	MX-80 (90 day)	MX-80 (1 year)
Porosity	67.2 %	65.5 %	64.3 %
Initial liquid pressure	−64 MPa	−55.5 MPa	−60.5 MPa
Retention curve	P_0 = 0.06 MPa λ_0 = 0.17 P_d = 500 MPa λ_d = 1	P_0 = 0.101 MPa λ_0 = 0.18 P_d = 500 MPa λ_d = 1.4	P_0 = 0.0985 MPa λ_0 = 0.17 P_d = 500 MPa λ_d = 1.4
Intrinsic permeability	8×10^{-19} m²	3.6×10^{-19} m²	3.4×10^{-19} m²
Relative permeability	$S_l^{5.7}$	$S_l^{5.4}$	$S_l^{5.7}$
Vapour diffusion tortuosity	0.5	1	
Thermal conductivity	Linear: 0 →1.3 W/mK		
Solid density	2 920 kg/m³	2 780 kg/m³	
Water density	1 000 kg/m³ (very low compressibility) $\alpha = 3.4 \times 10^{-4}$ °C⁻¹		
Initial temperature	24 °C		

The evaluated water retention curve was compared with an independently determined water retention curve for Asha 230B material, which was based on free swelling retention data presented by Johannesson et al. (2008) and the same void ratio as for the evaluated curve. The latter material is however of higher quality than the former, and this seems to explain the difference between the retention curves (Figure 2-4, left). Experimental data on hydraulic conductivity for different dry density vales for the same type of Asha material as used in this study is shown in Figure 2-4 (right). It can nevertheless be noted that the experimental data is much higher than the value evaluated in this study (see Chapter 5 for a brief discussion).

2.2.4 MX-80 roller-compacted pellets

A similar methodology was used for the adoption of two parameters sets for the MX-80 pellets, representing the conditions in test Cr3d (denoted "90 day model") and (Cr3e denoted "1 year model"), respectively.

The water retention curves were based on independently determined water retention data for free swelling samples and for two initial water contents: 10 % (Dueck and Nilsson 2010) and 17 % (Dueck 2004); and for the initial conditions in the two experiments. The initial water content was the same in the two tests (14.5 %), but the initial RH differed slightly with 66.5 % in test Cr3d and 64 % in test Cr3e. Extended van Genuchten water retention curves were adopted based on these data sets (Figure 2-5 and Table 2-3).

Saturation dependent permeability relations were calibrated by hand so that the resulting diffusivity relation exhibited a plateau at a sought level of 2.7×10^{-10} m^2/s (see Figure 2-6). The evaluated parameter values (k_0 and γ) are given in Table 2-3. It can be noted that the evaluated k_0 values (~3.5×10^{-19} m^2) were fairly similar to experimental data on hydraulic conductivity. For instance, the relation between void ratio and hydraulic conductivity for MX-80, evaluated by Åkesson et al. (2010), would yield a permeability level of 6–7×10^{-19} m^2 for the void ratio level used here.

Additional parameter values of relevance for this task in also compiled in Table 2-3. It should be noted that a vapour diffusion tortuosity value of 0.5 was used in the base case models (same as for the Asha model). In the modified models, this was however increased to the value of 1, since this was found to give results which were in a better agreement with the experimental data.

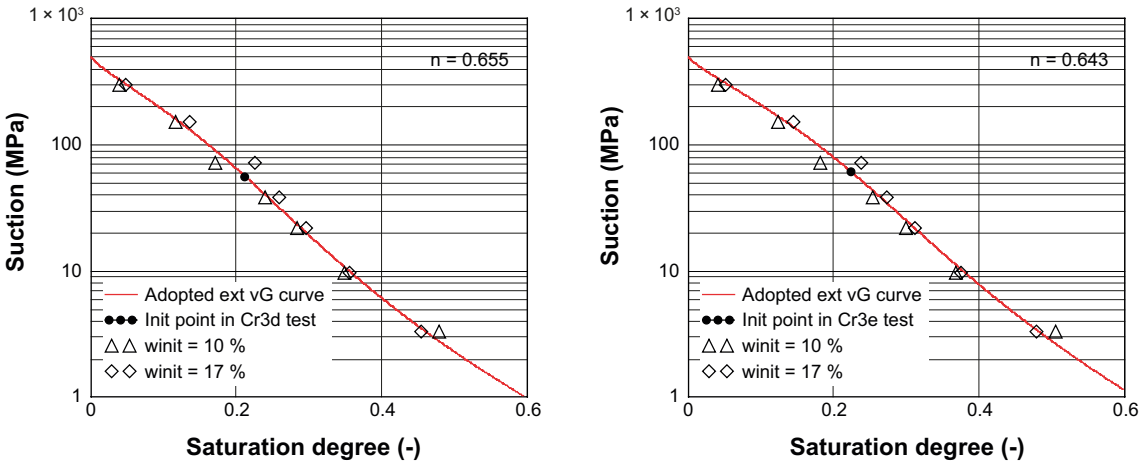

Figure 2-5. *Adoption of water retention curves for MX-80 pellets: 90 day model (left) and 1 year model (right).*

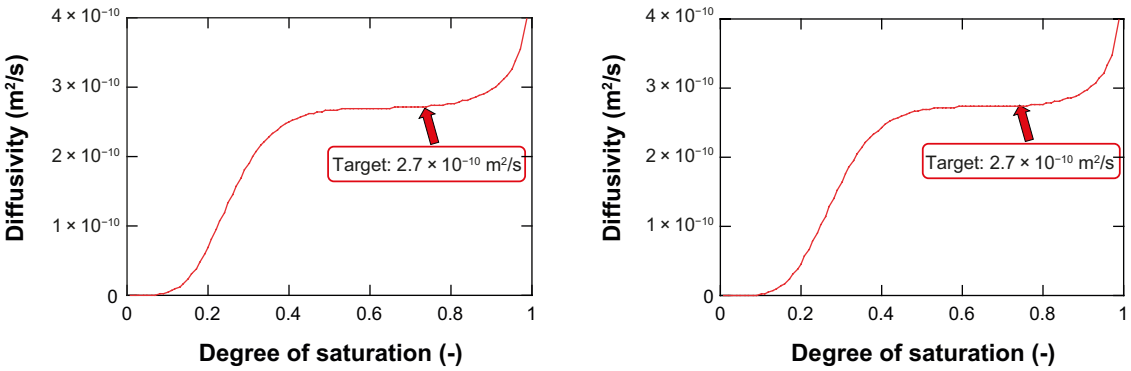

Figure 2-6. *Effective moisture diffusivity relation for MX-80 pellets, after calibration of permeability relations: 90 day model (left) and 1 year model (right).*

2.3 Model geometries and conditions

All analyzed Code_Bright models were based on a 1D geometry, 0.5 m long, and consisting of a single column of elements.

The models used for simulating the *A tests* generally had a hydraulic boundary with a specified 0.1 MPa liquid pressure which was increased from the initial suction value during the first (or 0.001) day and the temperature was generally kept at 24 °C. Three types of models were analyzed (Figure 2-7): i) a hydraulic (H) model with constant temperature; ii) a thermohydraulic model (TH) with constant temperature at the boundaries; and iii) a thermohydraulic model with initial water uptake, in which the liquid pressure in a 4 cm zone adjacent to the hydraulic boundary was increased from the initial value to 0.1 MPa during an initial period of 0.001 days, with the purpose of mimicking an initial water uptake of approximately 200 g. The analyzed models were discretized in either 20 or 50 elements.

The models used for simulating the *C tests* generally had closed hydraulic boundaries and thermal boundaries with 24 ºC at the cool side and 74 °C (increased from 24 to 74 °C during the first day) on hot side. Two types of models were analyzed (Figure 2-8): i) with a free temperature field, or ii) with a controlled temperature field. Three variants of controlled temperature fields were used, which corresponded to the measured results from the three tests.

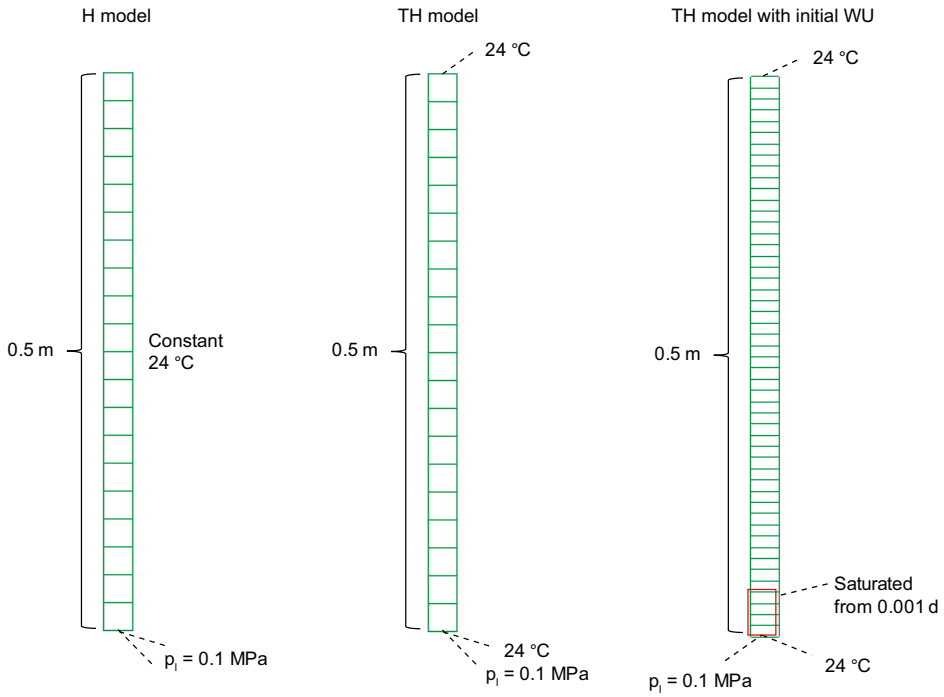

Figure 2-7. *Model geometry and boundary conditions for Test A models: without vapour (left), with vapour (center) and with vapour and initial water uptake (right).*

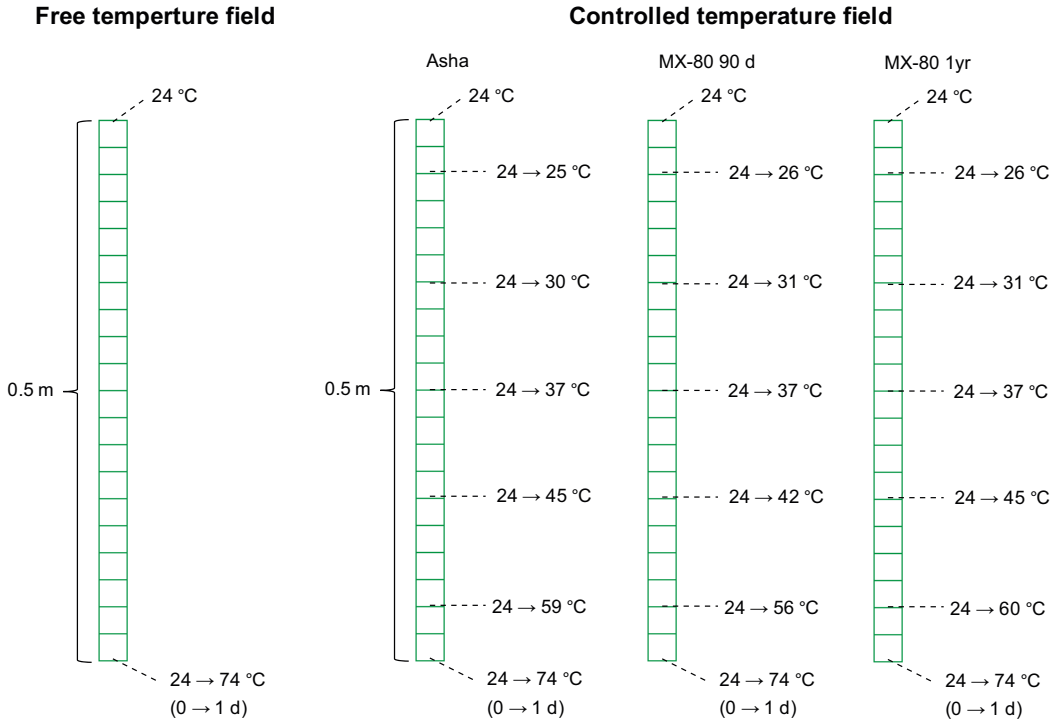

Figure 2-8. *Model geometry and conditions for Test C models: with free (left) and controlled (right) temperature field.*

3 Model results

3.1 Test A models

3.1.1 Asha

Two types of model results can be compared with experimental results for the A tests with Asha bentonite: water content profiles (for three different times) and water uptake.

The *H model* (without vapour diffusion) displayed a fairly good agreement with measured water content profiles (Figure 3-1, upper left), whereas the *TH model* (with vapour diffusion) was slightly better than H model regarding the spreading of the hydration front after 200 days (Figure 3-1, upper right). No evaluation of the water uptake was made for these models due to the major water uptake measured during the initial phase of the experiment (Ae3).

The calculated water content profiles for the *TH model with initial water uptake* were approximately the same as for the TH model regarding the data sets for 30 and 200 days (Figure 3-1, lower left). The model over-predicted the water contents regarding the results for 5 days however. The experiment for which these water contents were measured (Ae1) were on the other hand performed with the lower head (1–2 cm instead of 10 cm), and displayed a significantly lower initial water uptake (60 g instead of 200 g), and it may therefore not be relevant to compare the Ae1 data with this model. The modelled water uptake was evaluated as the sum of the initial water, calculated as the spatial integral of the increase in saturation degree after the initial time period (t_0), and the cumulative water uptake over the boundary, calculated as the time integral of the liquid and vapour mass fluxes ($\rho_w \cdot q_w$ and i_{vap}) at the boundary:

$$m(t_0) = \rho_w \cdot n \cdot A \cdot \int_0^L \left(S_l(x, t_0) - S_l^{init}\right) dx$$
$$m(t) = m(t_0) + A \cdot \int_{t_0}^{t} \left(\rho_w \cdot q_w(\tau) + i_{vap}(\tau)\right) d\tau \quad (3\text{-}1)$$

A comparison of modelled and measured uptake is shown (Figure 3-1, lower right), and it can be noted that the model (as expected) displayed the correct level (200 g) at the beginning of the tests. The subsequent modelled water uptake was however significantly lower than the measured uptake. The most likely cause of this deviation was that the measured water uptake data was influenced by different types of evaporation and leakage (see Åkesson et al. 2020).

3.1.2 MX-80

Three types of model results can be compared with experimental results for the A tests with MX-80 bentonite: water content profiles (for three different times), RH evolution (for three sensor positions) and water uptake.

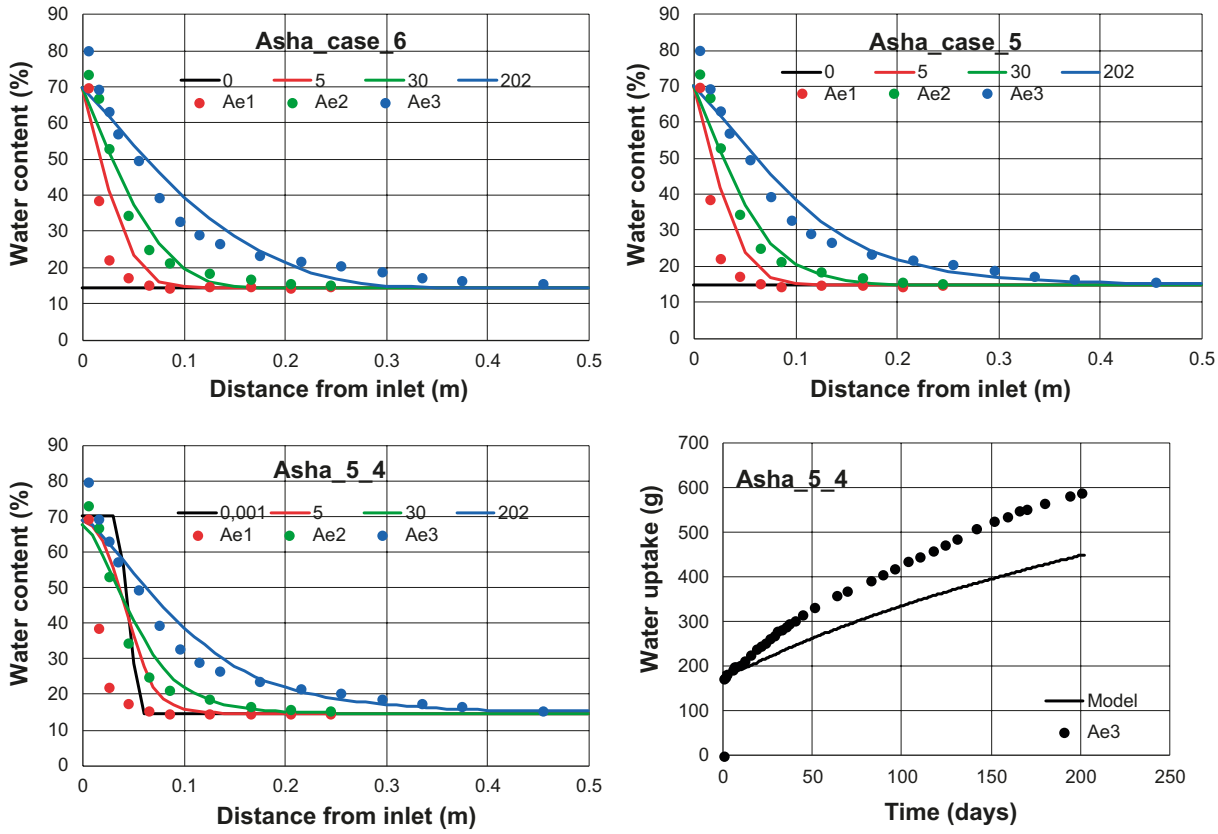

Figure 3-1. *Model and experimental results for A tests with Asha bentonite. Case without vapour (upper left), with vapour (upper right), and with vapour and initial water uptake (second row).*

As for the Asha cases, the *H model* (without vapour diffusion) displayed a fairly good agreement with measured water content profiles (Figure 3-2, upper left), whereas the calculated RH evolution, especially at the position 15.5 cm from the water inlet, was much slower than in the experiment (Figure 3-2, upper right). The water content profiles for the *TH model* (with vapour diffusion) were similar to the H model but slightly better regarding the spreading of the hydration front after 200 days (Figure 3-2, second row left). The calculated RH evolution for this model was significantly faster and in better agreement with experimental data (Figure 3-2, second row right). No evaluation of the water uptake was made for these models due to the major water uptake measured during the initial phase of the experiment (Ar3).

The calculated water content profiles for the *TH model with initial water uptake* were approximately the same as for the TH model regarding the data set for 200 days and to some extent also for the set for 30 days (Figure 3-2, third row left). The model clearly overpredicted the water contents regarding the results for 5 days however, presumably due to the same reason as noted for the Asha tests. The calculated RH evolution for this model was in better agreement with the experimental results, especially for the positions 3 cm and also 15.5 cm from the water inlet. Finally, a comparison of modelled and measured uptake is shown in Figure 3-2 (fourth row), and (as for the Asha case) it can be noted that the model displayed the correct level (200 g) at the beginning of the tests, whereas the subsequent modelled water uptake was significantly lower than the measured uptake.

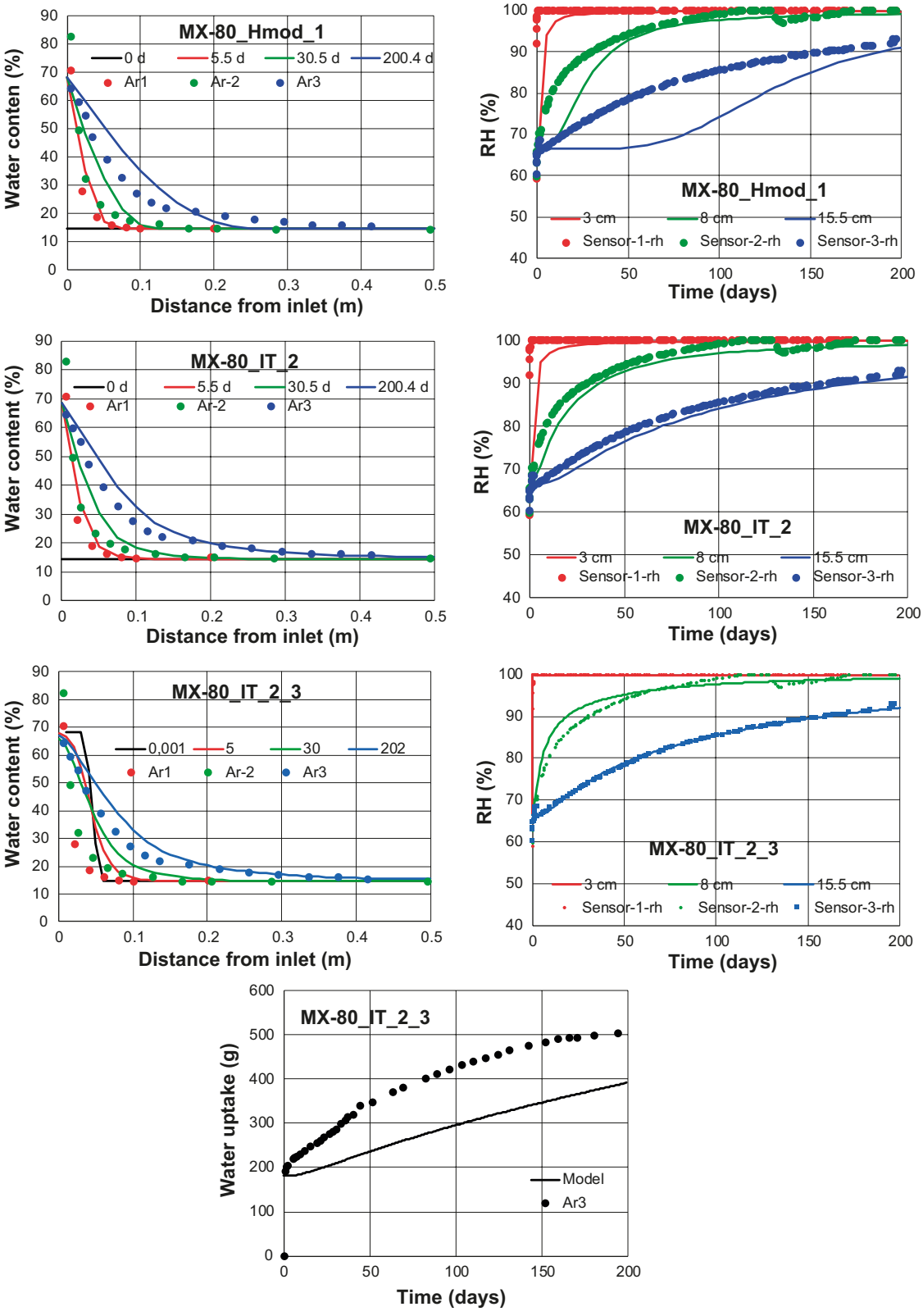

Figure 3-2. *Model and experimental results for A tests with MX-80 bentonite. Case without vapour (upper row), with vapour (second row), and with vapour and initial water uptake (third and fourth row).*

3.2 Test C models

Results for the models with Asha are shown in Figure 3-3, whereas results for the test cases with MX-80 is shown in Figure 3-4 and Figure 3-5 for tests run for 90 days and 1 year, respectively. Three types of results are compared: i) evolution of RH at sensor positions; ii) evolution of temperature at sensor positions; and iii) final water content distribution.

In general, a quite good agreement was found for all variables (RH, temperature and water content). The most noticeable difference was found for the temperature with the models with free temperature field: these models tended to overestimate the temperatures, especially in the warmer part, due to the absence of lateral heat loss in the model. This, in turn, tended to influence the moisture redistribution so that the water content and the RH levels were slightly lower along the warmer half of the test setup as compared with cases with controlled temperature field. This can especially be noted for the results for the test cases with Asha bentonite: see RH Sensor 1–3 (sensor positions are shown in Figure 1-1, right) and corresponding water content levels in Figure 3-3. To some extent it could also be noted for the test with MX-80 run for 90 days (see Sensor 2 in Figure 3-4).

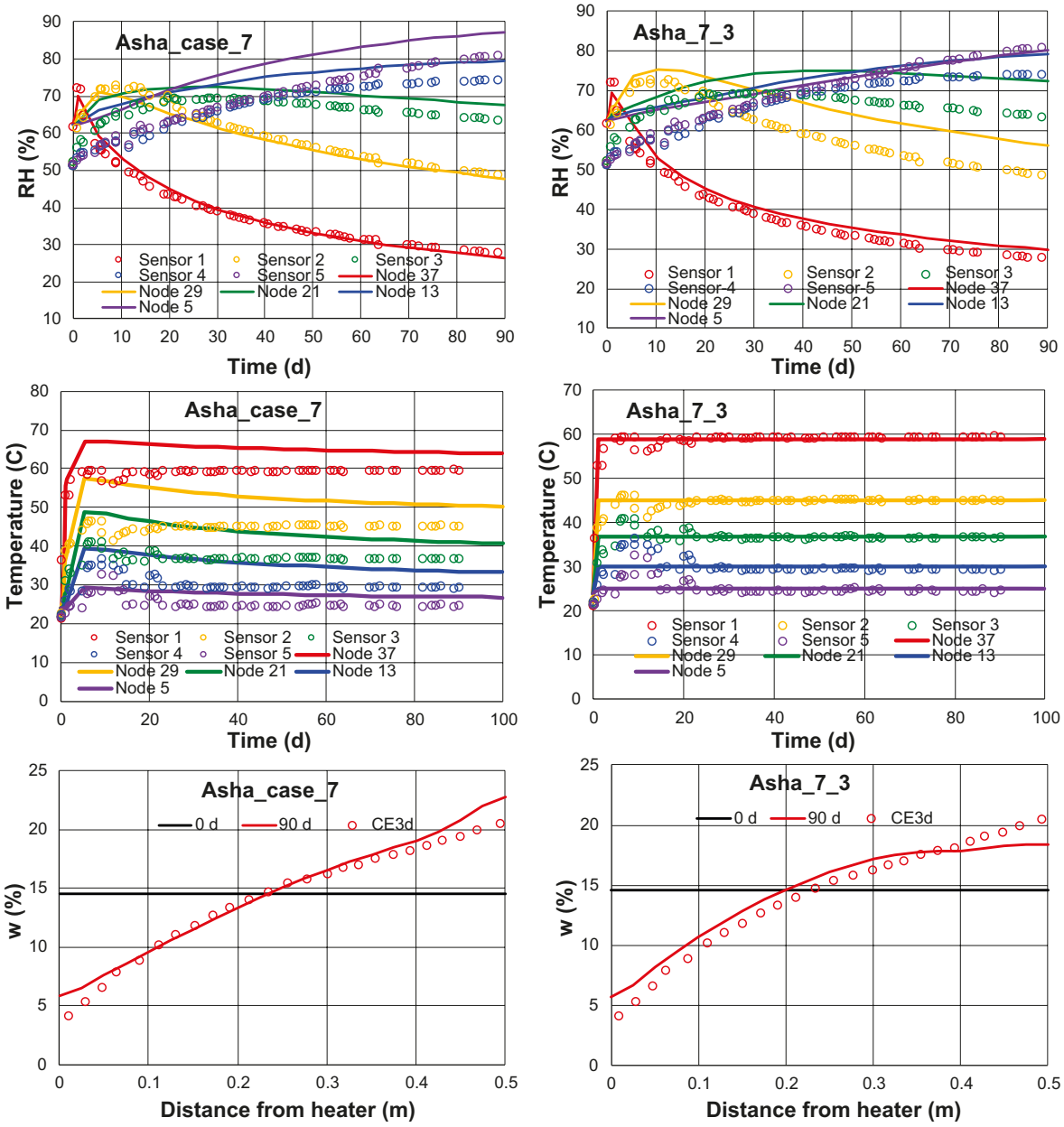

Figure 3-3. Model and experimental results for C tests with Asha bentonite. Case with free temperature field (left column) and controlled temperature field (right column).

The difference between cases with free and controlled temperature was less clear-cut in the test case with MX-80 run for 1 year. This appears to be due to the fact that the temperature levels in the models for this case are almost the same (Figure 3-5), which in turn probably was caused by the improved insulation in this test.

The timescales for the moisture redistribution and diverging RH levels were fairly well simulated, although the used vapour diffusion tortuosity values for the Asha pellets was only half the value as for the MX-80 pellets. This can possibly reflect the different pore-sizes in these materials.

The different tests displayed different behaviour regarding the early RH evolution. Especially the test with MX-80 run for 90 days displayed a distinct RH increase at the hot end, with values temporariliy above 90 %, not seen in the other two tests. The time to establish the final order of precedence of the different RH levels was also shorter in this test: 25 days (Figure 3-4) as compared with 40 days for the test with Asha (Figure 3-3) and 80 days for the test with MX-80 (1yr) (Figure 3-5). This difference was possibly caused by the modification of the insulation which was made for the latter of the two tests during the first few days of operation, and this may in turn have delayed the moisture redistribution.

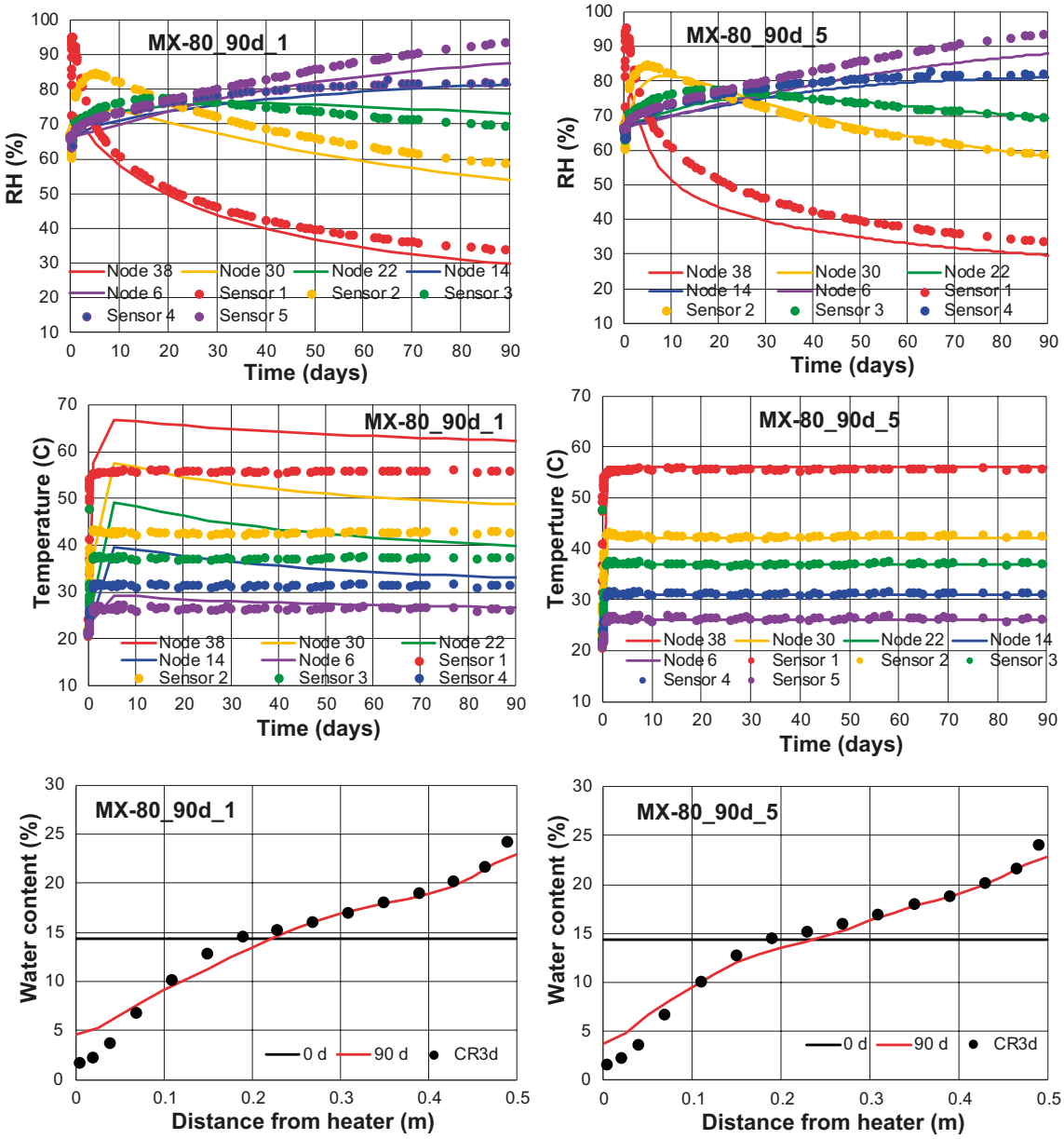

Figure 3-4. *Model and experimental results for C tests (90 days) with MX-80 bentonite. Case with free temperature field (left column) and controlled temperature field (right column).*

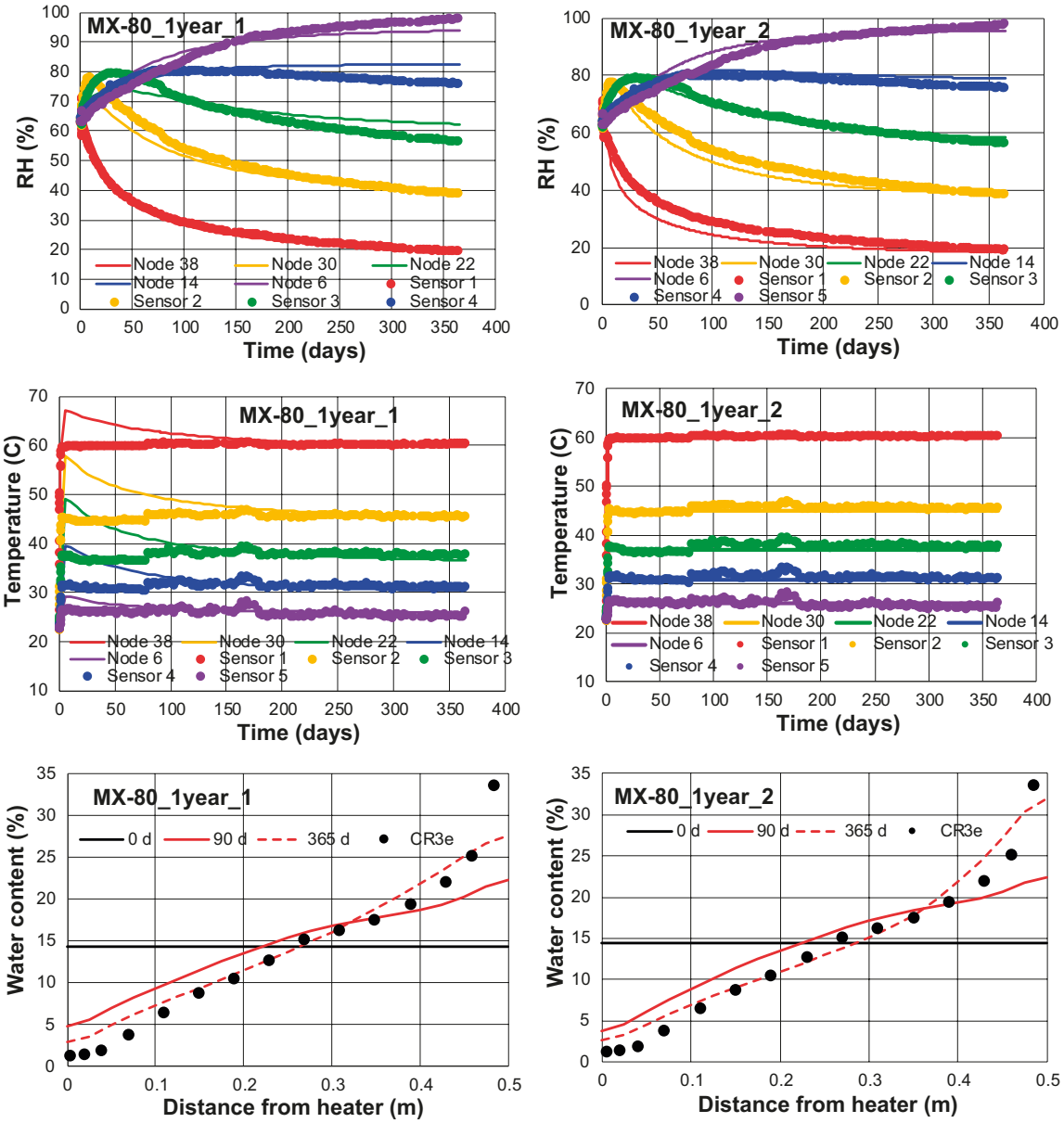

Figure 3-5. *Model and experimental results for C tests (one year) with MX-80 bentonite. Case with free temperature field (left column) and controlled temperature field (right column).*

4 Influence of vapour diffusion

The notion that the models are in better agreement with experimental data (especially the RH evolution in Figure 3-2) when vapour diffusion is included in the models calls for a more thorough understanding of the relative contribution of the different processes for the water transport.

The moisture diffusivity which is equivalent to the advective liquid flow driven by suction gradients is described by Equation (2-4). This is valid for isothermal conditions and for a homogenous porosity distribution. A corresponding expression for the diffusive vapour flow driven by gradient in vapour mass fraction can be formulated as (see Appendix A for a derivation):

$$D_v(S_l) = \frac{\rho_v}{\rho_w} \cdot (1 - S_l)\tau \cdot D_0 \frac{T^{2.3}}{P_g} \frac{M_w}{\rho_w RT} \frac{dP_l}{dS_l} \tag{4-1}$$

where ρ_v is the vapour density, ρ_w is the water density, τ is the vapour diffusion tortuosity, D_0 is a constant which corresponds to the diffusion of vapour in air (5.9×10^{-6} m^2 s^{-1} K$^{-2.3}$ Pa), T is the absolute temperature, P_g is the gas pressure, M_w is the molar weight of water, R is the general gas constant, and P_l is the liquid pressure.

Equation (2-4) and (4-1) are illustrated in Figure 4-1 for the parameter value set adopted for MX-80 (90 day) bentonite given in Table 2-3. This shows both the diffusivity value function for each of the two processes as well as the sum of these. It can be noted that vapour diffusion exceeds the contribution for advection below a saturation degree of 0.3–0.4. This means that the total diffusivity at the initial saturation degree is significantly higher than plateau level value of 2.7×10^{-10} m^2 s^{-1} which was adopted with the analytical solution (see Figure 2-2), and which was used as a target for the calibration of the permeability relations (Figure 2-6).

The equivalence between the two descriptions with i) advective liquid flow driven by suction gradients and diffusive vapour flow driven by gradient in vapour mass fraction; and ii) diffusive flow driven by gradients in the saturation degree, was verified with a numerical solution of the diffusion equation which was compared with the results from one of the Code_Bright models (MX-80_IT_2). The employed numerical solution is presented in Appendix B. The used parameter set was the same as MX-80 (90 day). The geometry was discretized in 40 elements. The number of time steps was 400. A comparison of the two models is shown in Figure 4-2. As expected, the results from two models are very similar which confirms that the two descriptions above are equivalent.

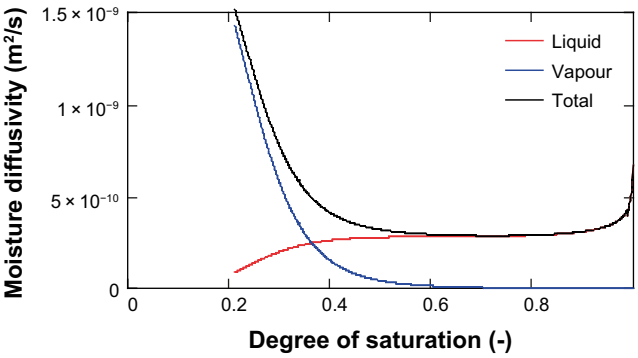

Figure 4-1. *Evaluated moisture diffusivity as a function of the degree of saturation.*

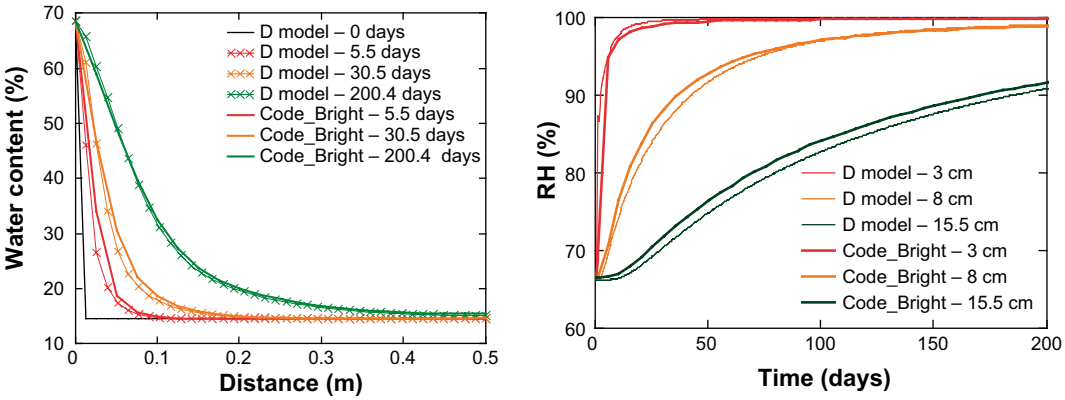

Figure 4-2. *Model results for A tests with MX-80. Diffusion model and Code_Bright model (MX-80_IT_2).*

5 Discussion

The processes in the A and C tests can essentially be described with the established thermohydraulic models. A summarizing assessment of the importance of the different parts of the material model for the different test conditions is shown in Table 5-1.

Table 5-1. Importance of different parts of the material model.

Model	Test A	Test C
Liquid transport	Major influence	Some influence
Vapour transport	Significant influence at low w	Major influence
Retention curve	Major influence	Major influence

The established thermohydraulic models are however insufficient to describe the processes in Test B conditions with specified liquid inflow rates. This is essentially a consequence of the occurrence of two pore systems with water: i) the interlayer pore space with water of hydration, which corresponds to the conventional properties regarding permeability and water retention curves; and ii) the macroscopic pore space with "free" water, which is characterized by much higher permeability levels and water activities or liquid pressures.

Two of the parameters used to describe the hydraulic processes, the intrinsic permeability and water retention curve, can ideally be determined from independent tests. The parameter values used for MX-80 were indeed found to be consistent with results from such tests. The previously analysed water retention curve for Asha material (Figure 2-4, left) was however performed on a bentonite quality which differs from the material used for the pellets in this study, which meant that those measurements could not be utilized. Moreover, the experimental data on the hydraulic conductivity (Figure 2-4, right) were found to differ significantly from the corresponding permeability value evaluated in this study, even though the material was the same. The very high hydraulic conductivity measured for this material appears to be caused by test conditions (e.g. piping) which are not representative for the conditions in the tests analysed here.

The saturation dependence of the relative permeability relation was stronger in these models (with exponent 5.4–5.7) in comparison to what is generally employed for compacted blocks (with exponent 3–4).

The measured temperatures in the C tests generally reflected the heat loss on the lateral sides of the test cylinder and displayed fairly constant trends. The latter observation was however contrasted by the models results which displayed decreasing trends which in turn was caused by the moisture redistribution and the linear saturation dependence of the thermal conductivity. This observation indicates that the actual saturation dependence is less pronounced than the one used in the model.

The potential influence of *gravity* was not investigated in this work. For the A tests, this was neglected since the pressure gradient in unsaturated bentonite greatly exceeds the specific weight of water. If the initial water-filling of the macro-pores close to the boundary would have been modelled explicitly together with the subsequent swelling and sealing of such pores, then this would obviously have been influenced by the gravity. Such processes have however been assigned to the modelling of the B tests (Åkesson et al. 2020) and was not included in the models of the A tests. For the C tests, the gravity was neglected due to the alignment of the test equipment and the temperature gradient in the vertical direction. However, if the *temperature gradient and the gravity vector would have been perpendicular,* it could very well be expected that this would influence the processes through natural convection. It should be valuable to investigate this more thoroughly, since such conditions are expected to occur in the buffer.

The potential influence of non-diffusive (advective) *gas transport* was not investigated in this work. Since the gas permeability in unsaturated pellets is very high, it can be expected that any gas pressure gradient, caused by either water uptake or heating, would immediately be equilibrated. Moreover, in the A tests the upper end of the cylinder was connected to a flexible balloon, thereby ensuring that the gas

pressure was maintained at atmospheric level. Nevertheless, in cases with *temperature gradients perpendicular to the gravity vector* it can be expected that natural convection will influence the processes which would call for the inclusion of gas transport in models.

The presented results from the A test suggest that a more refined procedure can be used for evaluating and back calculating the relevant *permeability relation*. A refined evaluation of the moisture diffusivity in which the saturation dependence is considered ($D(S_l)$) can be a useful starting point. Once a water retention curve is adopted, the diffusivity relation can be translated to a permeability relation, i.e $k \cdot k_r(S_l)$. Given the apparent importance of vapour diffusion at dry conditions, this evaluation may be refined by taking vapour diffusion coefficient $D_v(S_l)$ into account.

6 Concluding remarks

The presented modelling work has shown that the established TH models can essentially describe the processes in both the investigated test types.

The conditions in these tests are either defined by the pressure boundary (test type A), with essentially atmospheric pressure, or the temperature profile (test type C), which means that the processes are slow enough to sustain a thermodynamic equilibrium between the water activity in macro pores and in the interlayer clay water. This also means that the macro pores are essentially gas-filled as long as the bulk material is un-saturated, which in turn means that the water transport is governed by the same interlayer HM-mechanisms which determines the hydraulic conductivity at saturated conditions. This notion was generally supported by the fact that the used parameter values for MX-80 were consistent with results from independent test. It was however not valid for the hydraulic conductivity data for the Asha bentonite (see Figure 2-4, right), which probably was due to the test conditions in these measurements.

Equilibrium between the macro pores and the interlayers can however not be expected if the inflow rate is governed by external processes. This was the topic for the test type B, and a typical example of such a situation is the localized water inflow, through a fracture intersecting a deposition hole, into the pellets-filled slot. This will imply non-equilibrium between macro pores and the interlayers, which in turn can lead to water transport through the macro-pores.

Moreover, the presented models have shown that vapour transport governed by diffusion is a quite accurate and sufficient description of the processes in the investigated test types. However, this result may be due the situation in which the temperature gradient is parallel to the direction of gravity. If these vectors would be perpendicular, which is largely the case in the pellets-filled slot in a deposition hole, then it can be expected that the rate of vapour transport would increase due to natural convection.

References

SKB's (Svensk Kärnbränslehantering AB) publications can be found at www.skb.com/publications.

Dueck A, 2004. Hydro-mechanical properties of a water unsaturated sodium bentonite: laboratory study and theoretical interpretation. PhD thesis. Lund University, Sweden.

Dueck A, Nilsson U, 2010. Thermo-hydro-mechanical properties of MX-80. Results from advanced laboratory tests. SKB TR-10-55, Svensk Kärnbränslehantering AB.

Crank J, 1975. The mathematics of diffusion. 2nd ed. Oxford: Oxford University Press.

Johannesson L-E, Sandén T, Dueck A, 2008. Deep repository – engineered barrier system. Wetting and homogenization processes in backfill materials. Laboratory tests for evaluating modelling parameters. SKB R-08-136, Svensk Kärnbränslehantering AB.

Sandén T, Olsson S, Andersson L, Dueck A, Jensen V, Hansen E, Johnsson A, 2014. Investigation of backfill candidate materials. SKB R-13-08, Svensk Kärnbränslehantering AB.

Åkesson M, Börgesson L, Kristensson O, 2010. SR-Site data report. THM modelling of buffer, backfill and other system components. SKB TR-10-44, Svensk Kärnbränslehantering AB.

Åkesson M, Goudarzi R, Börgesson L, 2020. EBS TF – THM modelling. Water transport in pellets-filled slots. Laboratory tests and task description. SKB P-19-06, Svensk Kärnbränslehantering AB.

Appendix A

Vapour diffusion and moisture diffusivity

The water transport in bentonite can be described as a diffusive transport driven by gradients in the degree of saturation at isothermal conditions, and under the assumption that the porosity is homogenous. The water transport is thus described by the so-called moisture diffusivity. The transport coefficient for a suction gradient driven Darcy´s flow, i.e. the permeability and its saturation dependence $k(S_l)$, can easily be translated into a moisture diffusivity as: $D_l = k(S_l) \cdot n^{-1} \cdot \mu^{-1} \cdot dP_l/dS_l$, where n is the porosity, μ is the viscosity and dP_l/dS_l is the derivative of the water retention curve. This section describes a corresponding translation of the transport coefficient for diffusive vapour transport driven by gradients in vapour mass fraction (ω) into a moisture diffusivity.

The framework for this translation is illustrated in Figure A-1 which shows an element with section area A and thickness Δx, and with incoming and outgoing water mass fluxes.

The rate by which the mass of water changes in the element is thus equal to the difference between the flow rates in and out of the element:

$$A \cdot \Delta x \cdot n \cdot \frac{\partial(\rho_w S_l)}{\partial t} = A \cdot \left[j - \left(j + \frac{\partial j}{\partial x} \cdot \Delta x \right) \right] \tag{A-1}$$

which can be simplified as:

$$n \cdot \rho_w \frac{\partial S_l}{\partial t} = -\frac{\partial j}{\partial x} \tag{A-2}$$

The mass flux j is here identified with the diffusive vapour mass flux j_v as implemented in Code_Bright:

$$j_v = -\rho_g \cdot n(1 - S_l)\tau \cdot D_0 \frac{T^{2,3}}{P_g} \frac{\partial \omega}{\partial x} \tag{A-3}$$

The vapour mass fraction gradient is developed in terms of a gradient in the saturation degree:

$$j_v = -\rho_g \cdot n(1 - S_l)\tau \cdot D_0 \frac{T^{2,3}}{P_g} \frac{d\omega}{dP_v} \frac{dP_v}{dP_l} \frac{dP_l}{dS_l} \frac{\partial S_l}{\partial x} \tag{A-4}$$

Fick´s second law can be described in terms of saturation degrees in the following form:

$$\frac{\partial S_l}{\partial t} = \frac{\partial}{\partial x}\left(D \frac{\partial S_l}{\partial x} \right) \tag{A-5}$$

The approach is thus to equate the mass balance (A-2) and the mass flux (A-4) with Fick´s second law (A-5) and from this identify an expression for the moisture diffusivity D.

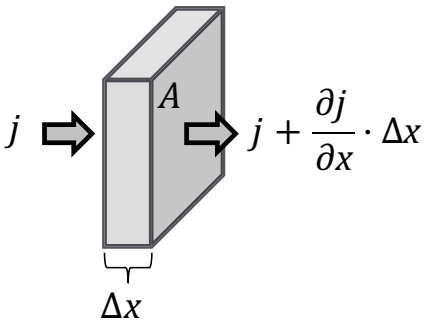

Figure A-1. *Fluxes in and out of element.*

The first derivative in Equation (A-4) is evaluated from the general gas law as:

$$\omega \approx \frac{P_v}{P_g}\frac{M_w}{M_a} \quad \rightarrow \frac{d\omega}{dP_v} \approx \frac{M_w}{P_g M_a} \tag{A-6}$$

The second derivative can be evaluated from Kelvin´s equation:

$$P_v = P_v^{sat} \cdot exp\left[\frac{(P_l - P_g)M_w}{\rho_w RT}\right]$$

$$\rightarrow \frac{dP_v}{dP_l} = P_v^{sat} \cdot \frac{M_w}{\rho_w RT} exp\left[\frac{(P_l - P_g)M_w}{\rho_w RT}\right] = \frac{M_w}{\rho_w RT} \cdot P_v \tag{A-7}$$

Together, these two derivatives can be expressed as:

$$\frac{d\omega}{dP_v}\frac{dP_v}{dP_l} = \frac{M_w}{\rho_w RT} \cdot \frac{P_v M_w}{P_g M_a} = \frac{M_w}{\rho_w RT}\frac{\rho_v}{\rho_g} \tag{A-8}$$

Taken together, the moisture diffusivity can be identified as:

$$D_v = \frac{\rho_v}{\rho_w} \cdot (1 - S_l)\tau \cdot D_0 \frac{T^{2,3}}{P_g}\frac{M_w}{\rho_w RT}\frac{dP_l}{dS_l} \tag{A-9}$$

Appendix B

Numerical scheme for water-uptake calculations

A numerical scheme was prepared in which the water transport was described by a saturation dependent moisture diffusivity function D(S), and the diffusion equation was solved with an explicit finite-difference method. The motive for this was to verify the equivalence between the descriptions with: i) advective liquid flow driven by suction gradients and diffusive vapour flow driven by gradient in vapour mass fraction; and ii) diffusive flow driven by gradients in the saturation degree. The scheme was implemented in the MathCad software.

The 1D geometry of the water-uptake tests are discretized in n elements according to Figure B-1 (left). The index *i*, with values between 0 and n−1, denote the element. The width of each element is Δx = L/(n−1), except for the inner and outer elements which have half this width. The numerical scheme used to calculate the saturation profile for a point in time, with index *j*, is illustrated in Figure B-1 (right). The time step between two successive point in time is denoted Δt.

The diffusion equation can be developed in the following three terms:

$$\frac{\partial S_l}{\partial t} = \frac{\partial}{\partial x}\left(D\,\frac{\partial S_l}{\partial x}\right) = D\,\frac{\partial^2 S_l}{\partial x^2} + \frac{\partial D}{\partial x}\cdot\frac{\partial S_l}{\partial x} \tag{B-1}$$

These terms with partial derivatives are estimated with the following corresponding finite differences:

$$\begin{cases} \dfrac{\partial S_l}{\partial t} & \approx & \dfrac{S_l^{j,i} - S_l^{j-1,i}}{\Delta t} \\ D\,\dfrac{\partial^2 S_l}{\partial x^2} & \approx & D(S_l^{j-1,i})\cdot\dfrac{S_l^{j-1,i+1} - 2S_l^{j-1,i} + S_l^{j-1,i-1}}{\Delta x^2} \\ \dfrac{\partial D}{\partial x}\cdot\dfrac{\partial S_l}{\partial x} & \approx & \dfrac{D(S_l^{j-1,i+1}) - D(S_l^{j-1,i-1})}{2\cdot\Delta x}\cdot\dfrac{S_l^{j-1,i+1} - S_l^{j-1,i-1}}{2\cdot\Delta x} \end{cases} \tag{B-2}$$

Note that the axial position of element *i* is expressed as i·Δx. For convenience, the following constant is defined:

$$X = \frac{\Delta t}{\Delta x^2} \tag{B-3}$$

Based on Equations (B-1) – (B-3), the following expression can be derived for the saturation degree in all elements, except for the inner and outer elements:

$$S_l^{j,i} = S_l^{j-1,i} + X\cdot D\left(S_l^{j-1,i}\right)\cdot\left[S_l^{j-1,i+1} - 2S_l^{j-1,i} + S_l^{j-1,i-1}\right] + \frac{X}{4}\cdot\left[D(S_l^{j-1,i+1}) - D(S_l^{j-1,i-1})\right]\cdot\left[S_l^{j-1,i+1} - S_l^{j-1,i-1}\right] \tag{B-4}$$

The saturation degree of the first element is given as a boundary condition, which is full saturation ($S_l^{j,0} = 1$), and for the last element (i = n−1) this is the same as for the adjacent element ($S_l^{j,n-1} = S_l^{j,n-2}$).

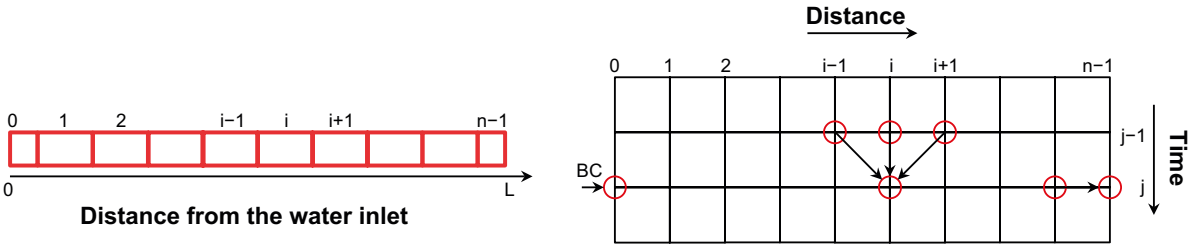

Figure B-1. *Discretization of geometry in n elements with index i, shown as red boxes (left). Numerical scheme used to update the saturation profile (right). Points in time are denoted with index j.*

Arkitektkopia AB, Bromma, 2020

SKB is responsible for managing spent nuclear fuel and radioactive waste produced by the Swedish nuclear power plants such that man and the environment are protected in the near and distant future.

skb.se